14

Characterization of Delamination Failure

The interlaminar mode of fracture (delamination) has aroused considerable attention since the early 1970s [1]. With the introduction of laminated composites into structures subjected to service loads, it has become apparent that the delamination failure mode has the potential for being the major life-limiting failure process. These delaminations are typically induced in composite laminates during service. However, delaminations may also be introduced during processing of the lay-up, for example as a result of contamination of the prepreg, leading to locally poor ply adhesion, or they may form locally in regions of high void content. Delamination may also be introduced during post-fabrication handling of the structure.

It is recognized that a delamination represents a crack-like discontinuity between the plies and that it may propagate during application of mechanical or thermal loads, or both. It thus seems appropriate to approach the delamination using fracture mechanics (Section 2.7), which indeed has evolved as a fruitful approach for material selection and assessment of structural integrity. Fracture mechanics of delaminations is commonly based on the strain energy release rate, and fracture toughness is expressed as the work of fracture. Consequently, many new fracture tests have been devised for measuring the static interlaminar fracture toughness, as well as the crack propagation rate during cyclic loading. Most such tests and standard test procedures are limited to unidirectional $[0]_n$ laminates in which a delamination propagates between the plies along the fiber direction. In laminates with multidirectional plies, the crack may have a tendency to branch through the neighboring plies, invalidating the coplanar assumption in fracture analysis [2–4]. Composites with tough resin films (called interleaves) between the plies may experience peculiar delamination resistance behavior depending on crack path selection, i.e., if the crack propagates cohesively in the tough interlayer or adhesively at the film–composite interface [5]. In woven fabric composites, a delamination crack will interact with matrix regions and interlacing yarns during its propagation, and as a result, will experience varying growth resistance [6]. Composites with through-thickness reinforcement may experience large extended regions where the reinforcements bridge the crack (bridging zones), which invalidates data reduction schemes based on linear elastic fracture mechanics [7]. Although fiber bridging is common in unidirectional (all 0° plies) composites, characterization of the delamination

resistance of such composites tends to be associated with fewer complications. Consequently, we will here limit attention to unidirectional composites.

Fracture mechanics analysis, preparation of test specimens, testing, and data reduction will be described for some contemporary interlaminar fracture test specimens, namely, the double-cantilever beam (DCB) specimen (Mode I), end-notched flexure (ENF) specimen (Mode II), four-point bend end-notched flexure (4ENF) specimen (Mode II), the mixed-mode bending (MMB) specimen, and the edge crack torsion (ECT) specimen (Mode III). The various fracture modes are defined in Figure 2.9.

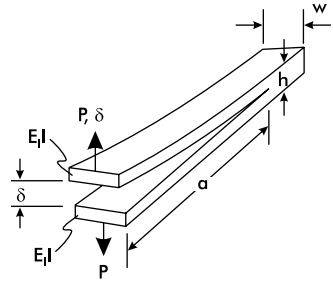

FIGURE 14.1
DCB specimen geometry.

14.1 Double-Cantilever Beam (DCB) Test

The DCB specimen for Mode I fracture testing and the test principle is shown in Figure 14.1. This specimen is a standard test method, ASTM D 5528 [8]. The purpose of the test is to determine the opening mode interlaminar fracture toughness, G_{IC}, of continuous fiber composite materials with a polymer matrix. First developed in a tapered form by Bascom, et al. [9], the straight-sided geometry proposed by Wilkins et al. [10], shown in Figure 14.1, has become standard. Although data reduction does not rely on the classical beam theory approach used by Wilkins, et al. [10], the simplicity of this theory makes it easy to examine some features of the DCB specimen.

If we assume that classical beam theory is valid, the load-point compliance, $C = \delta/P$, of the DCB specimen becomes

$$C = \frac{2a^3}{3E_1 I} \tag{14.1}$$

where P is the load applied, δ is the crack opening, a is the crack length, and E_1I is the flexural rigidity of each beam of the specimen, with E_1 being the Young's modulus of the composite in the fiber direction and I the moment

of inertia (Figure 14.1). The strain energy release rate, $G = G_I$, is obtained from Equation (2.59)

$$G = \frac{P^2}{2w}\frac{dC}{da} \tag{14.2}$$

in which w is the specimen width. Equations (14.1) and (14.2) give

$$G = \frac{P^2 a^2}{wE_1 I} \tag{14.3}$$

If G_{IC} is a true material constant, stable crack growth requires (see Section 2.7),

$$dG/da \leq 0 \tag{14.4}$$

For the DCB specimen under fixed-load conditions, dG/da is obtained from Equation (14.3) as

$$\frac{dG}{da} = \frac{2P^2 a}{wE_1 I} \tag{14.5}$$

This quantity is always positive and thus the crack growth is unstable under load-controlled testing conditions.

For fixed-grip conditions, dG/da may be obtained by substitution of $P = \delta/C$ in Equation (14.2) and differentiation

$$\frac{dG}{da} = \frac{-4\delta^2 a}{c^2 wE_1 I} \tag{14.6}$$

This quantity is always negative, and thus the crack growth is stable. Experimentally, most testing is performed under fixed-grip conditions (displacement control), which should render stable crack growth.

14.1.1 DCB Specimen Preparation and Test Procedure

The DBC specimen should be at least 125 mm long and between 20 and 25 mm wide. The number of plies, dimensions, and preparation of the panel are outlined in Appendix B. An even number of plies should be employed to achieve a thickness (h in Figure 14.1) between 3 and 5 mm. Variations in thickness should be less than 0.1 mm. Tough composites may require thicker specimens to avoid large displacements and nonlinear response. Figures 14.2 and 14.3 show the DCB specimen with hinge loading tabs prepared and

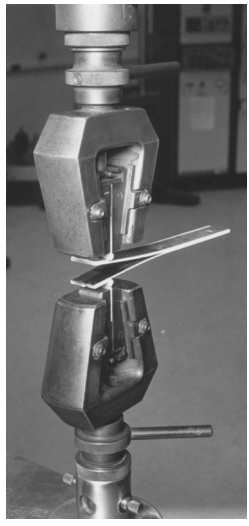

FIGURE 14.2
DCB test setup.

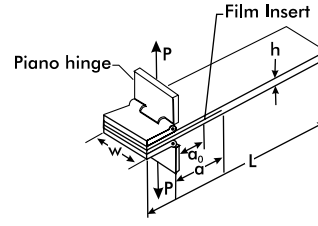

FIGURE 14.3
Hinge loading tab arrangement for the DCB specimen.

bonded as described in Chapter 4. The precrack is defined by inserting a thin film (<13 μm) at the midplane of the panel (see Appendix B). Crack length, a, is defined as the distance from the line of load application to the crack tip, Figure 14.3. The length of the film insert should be adjusted to obtain a precrack length, a_0, of approximately 50 mm (see Appendix B).

Measure thickness and width of the specimen close to each end and at the center and calculate averages. Paint the specimen edges with a thin, white, brittle coating such as typewriter correction fluid. To aid in recording of crack length, mark the first 5 mm from the insert with thin vertical lines every 1 mm. Mark the remaining 20 mm every 5 mm.

The specimen should be mounted in the grips of a properly calibrated test machine with a sufficiently sensitive load cell. A traveling optical microscope with approximately 10× magnification and a cross hair can be positioned on one side of the specimen to enable monitoring of the delamination crack tip and its extension during the fracture test within ±0.5 mm. Locate the cross hair at the delamination front without applying load to the specimen to obtain a record of the precrack length, a_o (Figure 14.3). Set the crosshead rate at 0.5 mm/min, and plot load vs. crosshead displacement for real-time visual inspection of the load-displacement response. Displacement of the loaded ends (δ in Figure 14.1) can be taken as the crosshead travel, provided the machine and load cell are stiff enough not to deform more than 2% of the total opening displacement.

Observe the delamination front as the specimen is being loaded. When the delamination begins to grow from the end of the insert, mark this incident as a_o on the chart recording as indicated in Figure 14.4. Continue to observe the front of the growing crack, and mark the chart accordingly.

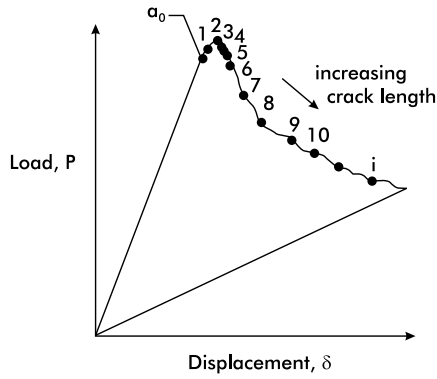

FIGURE 14.4
Schematic load-displacement record during crack growth for a DCB test.

For the first 5 mm of crack growth, each 1 mm increment should be marked. After 5 mm of crack extension, the crosshead rate may be increased. Mark every 5 mm of crack length on the graph. Observe the opposite edge to monitor deviations from uniform crack extension across the beam width. The difference in crack length between the two edges should be less than 2 mm for a valid test. When the delamination has extended about 25 mm, the specimen may be unloaded while the unloading load-displacement response (see Figure 14.4) is recorded. A common occurrence in testing unidirectional DCB specimens is fiber bridging, which refers to debonded fibers bridging the fracture surfaces, as illustrated in Figure 14.5. The fiber bridging elevates the fracture resistance as a result of the closure tractions that develop in the fibers that bridge the crack faces behind the crack tip, and the energy consumed as the bridged fibers debond from the matrix [11].

It is common to display the fracture toughness measured at various crack lengths as a resistance curve (R-curve). As discussed by Suo et al. [11], such R-curves do not represent true material behavior because they depend on specimen thickness. Fiber bridging is less likely to occur in multidirectional laminates used in composite structures because less opportunity exists for fiber wash, i.e., intermingling of wavy fibers between adjacent plies. Fiber bridging is thus likely to lead to nonconservative estimates of the actual delamination toughness. It is argued that the most meaningful, and also conservative, estimate of fracture toughness is the initiation toughness, G_{IC}(init.), associated with the initial crack propagation from the Teflon insert [8], because this value is not influenced by fiber bridging. Further discussion will follow.

14.1.2 DCB Data Reduction

Several data reduction methods for evaluating the Mode I fracture toughness, G_{IC}, have been proposed [12]. A simple, yet accurate method is the

empirical compliance method suggested originally by Berry [13], where the beam compliance, $C = \delta/P$, is expressed as a power function of crack length,

$$C = \frac{a^n}{H} \tag{14.7}$$

where a is the crack length, and n and H are parameters determined experimentally. If classical beam theory and the assumption of fixed ends are valid, $n = 3$ and $H = 3E_1I/2$. In reality, the legs of the DCB specimen are elastically built into the uncracked portion of the specimen rather than being rigidly fixed. This will cause deviations from classical beam theory.

To establish the actual values of the empirical parameters in Equation (14.7), measured load and displacement data at each crack length are evaluated from the load-displacement graph (Figure 14.4), and the stiffness, i.e., the inverse of the compliance ($1/C = P_c/\delta_c$), is plotted vs. crack length (a) in a double-logarithmic graph as shown in Figure 14.6. By fitting a straight line to the data, it is possible to establish the exponent, n, in Equation (14.7). Substitution of Equation (14.7) into (14.2) yields at fracture

$$G_{IC} = \frac{nP_c\delta_c}{2wa} \tag{14.8}$$

in which P_c and δ_c are the critical load and displacement associated with each crack length, a.

Three toughness values corresponding to crack growth from the insert may be defined. G_{IC}(NL) refers to the critical load and displacement associated with the deviation from linear response (Figure 14.4). The second definition, G_{IC}(vis.), refers to the visual observance of crack growth measured with the traveling microscope. The third definition, G_{IC}(5%), uses the load

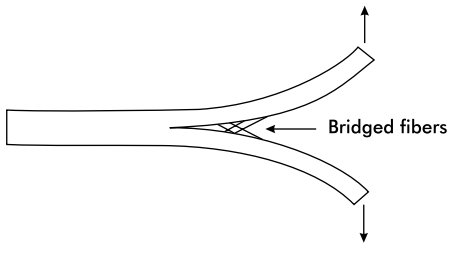

FIGURE 14.5
Fiber bridging in DCB testing.

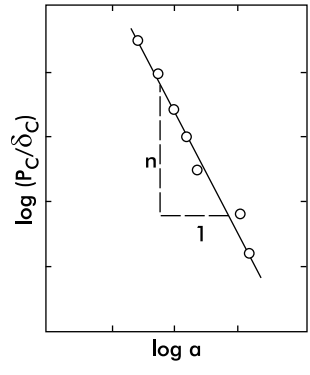

FIGURE 14.6
Log–log plot of DCB specimen stiffness vs. crack length.

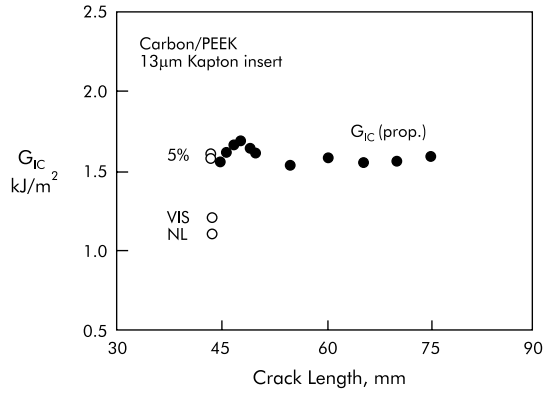

FIGURE 14.7
R-curve describing mode I interlaminar fracture resistance of carbon–PEEK with a 13 μm insert.

and displacement at a 5% increase in compliance. G_{IC}(NL) is typically the most conservative estimate of the fracture toughness and is recommended as a measure of Mode I delamination toughness. For subsequent crack growth, G_{IC} is calculated from Equation (14.8) using the recorded loads and crack lengths (Figure 14.4).

A crack growth resistance curve (R-curve) displaying G_{IC} vs. crack extension can be constructed from the fracture toughness, G_{IC}, and crack length, a, data. Figure 14.7 shows an example of an R-curve for a carbon/polyetheretherketone (PEEK) composite. At the first loading increment, the delamination grows from the tip of the thin film insert starter crack without any influence from fiber bridging. The corresponding three initiation fracture toughness values, G_{IC}(NL), G_{IC}(vis.), and G_{IC}(5%), are indicated in Figure 14.7. As the crack grows, the crack surfaces become more and more separated and bridged fibers may fracture or become pulled out from the matrix, which causes the apparent fracture toughness to increase. With further crack extension a steady-state toughness, G_{IC}(prop.), is usually reached, corresponding to an equilibrium number of bridged fibers per unit crack area. As mentioned earlier, the initial value associated with propagation of the crack from the film insert constitutes a well-defined measure of fracture toughness because it is unaffected by the fiber bridging that occurs with crack extension [11,12].

14.2 End-Notched Flexure (ENF) Test

The ENF specimen (Figure 14.8) was introduced as a pure Mode II delamination specimen for testing of composites by Russell and Street [14]. The purpose of the ENF specimen is to determine the critical strain energy release rate in pure Mode II loading of unidirectional composites [14,15]. The ENF specimen

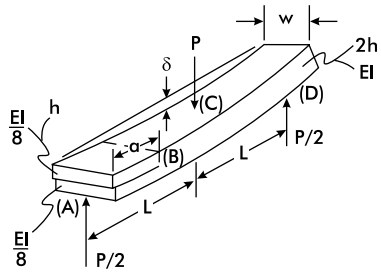

FIGURE 14.8
ENF specimen.

produces shear loading at the crack tip without introducing excessive friction between the crack surfaces [16,17]. The ENF specimen is standardized in Europe [18] and Japan [19], and has been studied extensively in the U.S. by the ASTM D-30 Committee as a candidate for ASTM standardization. As will be discussed, however, the ENF specimen is inherently unstable under displacement control, which has slowed acceptance of this specimen as a standard fracture test.

Assuming that classical beam theory is valid, an expression for the strain energy release rate, G, can be derived [14,15]:

$$G = \frac{9P^2Ca^2}{2w(2L^3 + 3a^3)} \tag{14.9}$$

where P is the applied load, C is the compliance, a is the crack length, w is the specimen width, and L is the span between the central loading cylinders and the outer support cylinders (Figure 14.8). The specimen compliance as given by beam theory [14,15] is

$$C = \frac{2L^3 + 3a^3}{8E_1wh^3} \tag{14.10}$$

where E_1 is the flexural modulus, and h is one half the total thickness of the beam, i.e., the thickness of each sub-beam of the delaminated region.

The stability of crack growth may be judged from the sign of dG/da. For fixed-load conditions, Equations (14.9) and (14.10) give

$$\frac{dG}{da} = \frac{9aP^2}{8Ew^2h^3} \tag{14.11}$$

This quantity is positive, hence the crack growth is unstable.

For fixed-grip conditions, Equations (14.9) and (14.10) give

$$\frac{dG}{da} = \frac{9\delta^2 a}{8E_1w^2h^3C^2}\left[1 - \frac{9a^3}{2L^3 + 3a^3}\right] \tag{14.12}$$

Stable crack growth requires dG/da to be less than or equal to zero. This gives

$$a \geq L/\sqrt[3]{3} \approx 0.7L \tag{14.13}$$

Consequently, for the commonly used a = L/2, the crack growth is unstable also under fixed-grip conditions. This has the consequence that only one measurement of the fracture toughness is obtained for each specimen.

14.2.1 ENF Specimen Preparation and Test Procedure

The ENF specimen is typically 120 mm long and 20 to 25 mm wide. Specimen thicknesses for unidirectional carbon- and glass-fiber composites are typically 3 and 5 mm (60% fiber volume fraction), respectively. The specimen is loaded in a three-point bend fixture (Figure 14.9) with a distance between the supports, 2L, of 100 mm. The loading and support cylinders should be about 5 mm in diameter. The crack length-to-half span ratio, a/L, should be 0.5 at propagation of the crack. Panels should be prepared with a nonadhesive Teflon or Kapton film of thickness less than 13 μm placed at the midplane to define a starter crack. Further details of specimen preparation are presented in Appendix B. After specimens have been cut from the panel, the width and thickness at the center and 1 cm from each end should be measured for all specimens. The thickness variations should not exceed 0.1 mm. Prior to testing, a brittle white coating should be applied to the specimen edges as described in Section 14.1.1.

The issue of whether precraking of the ENF specimen should be performed has long been discussed. Precracking in Mode I is likely to create the fiber-bridging discussed in Section 14.1, and is not recommended [20]. A shear precrack may be achieved by loading the specimen in the stable crack length regime, a >0.7L, according to Equation (14.13), until a short extension of the crack occurs. Unfortunately, however, it is difficult to detect the exact position and shape of the shear precrack after completion of the fracture test, and it is also difficult to obtain a straight and uniform crack front. For reasons of simplicity and consistency with the DCB procedure (Section 14.1), crack propagation from specimens with thin insert films, but without additional extension of the precrack, is advocated.

The ENF specimen is placed in a standard three-point bend fixture [21], so that a crack length, a, of 25 mm is achieved (Figures 14.9 and 14.10). To facilitate appropriate positioning of the crack tip, a low-magnification (10×) traveling microscope is useful. Mark the support location on the specimen edge for subsequent measurement of crack length. Measure the center beam deflection (load-point displacement), δ, with a linear variable differential transformer (LVDT), or from the crosshead displacement corrected for the machine compliance. Use a crosshead rate in the range of 0.5 to 1 mm/min, and monitor the load-displacement response. Record both loading and

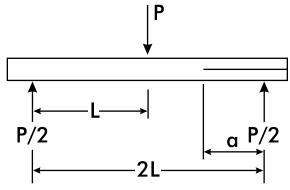

FIGURE 14.9
ENF specimen geometry parameters.

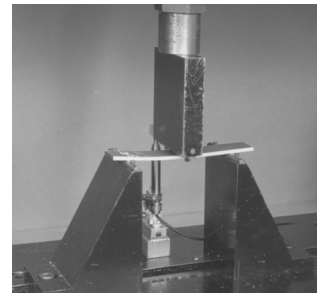

FIGURE 14.10
ENF test setup.

unloading paths. Observe the crack tip during loading (a traveling microscope is recommended) to detect any slow, stable crack propagation prior to fast fracture. Slow crack propagation preceding fast fracture is commonly observed in ductile matrix composites and leads to a nonlinear load-displacement curve (Figure 14.11 [22]). Indicate this event on the load-deflection curve. An example of a load-deflection curve for a brittle carbon/epoxy composite is shown in Figure 14.12. For this composite, fast fracture occurred without noticeable stable crack extension, and the response curve is essentially linear up to fracture.

14.2.2 ENF Data Reduction

Evaluation of the Mode II fracture toughness, G_{IIC}, requires a record of the load-displacement response, e.g., Figures 14.11 and 14.12. Toughness values G_{IIC}(NL), G_{IIC}(vis.), and G_{IIC}(max.), referring to the loads at the onset of nonlinearity, visual stable crack extension, and maximum load, respectively,

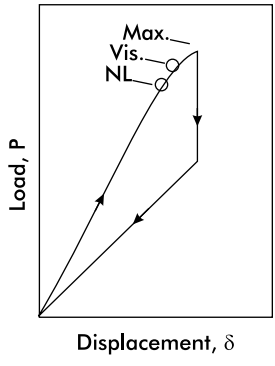

FIGURE 14.11
Schematic load-displacement curve for ENF fracture test of a ductile matrix composite. P(NL), P(vis.), and P(max.) denote loads at onset of nonlinearity, onset of visible stable crack growth, and onset of fast fracture, respectively.

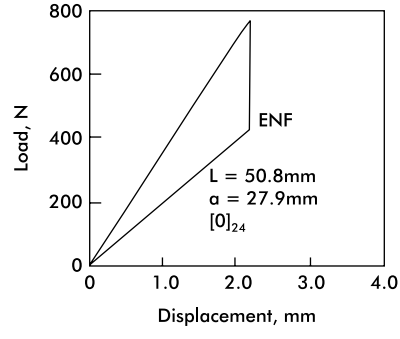

FIGURE 14.12
Load-deflection curve for a carbon/epoxy (AS4/3501-6) ENF specimen. L = 50.8 mm, w = 25.4 mm, and a = 27.9 mm.

as illustrated in Figure 14.11, can be determined. For calculation of G_{IIC}, the initial crack length is required. The initial crack length can be measured by cracking the failed specimen into two parts and measuring the distance between the support cylinders (marked on the specimen edge) and the initial crack front at three locations (each edge and center of the beam width). Commonly, the support cylinders leave imprints on the specimen surface that can be used to further verify the crack length measurements after the fracture test.

If the flexural modulus, E_1, of the specimen is not known, the fracture toughness, G_{IIC}, is calculated from the following beam theory expression using the measured compliance, C,

$$G_{IIC} = \frac{9a^2P^2\left(C - C_{SH}\right)}{4wL^3\left[1 + 1.5\left(a/L\right)^3\right]} \tag{14.14}$$

where C_{SH} is a compliance correction factor arising from interlaminar shear deformation calculated from

$$C_{SH} = \frac{6L + 3a - L^3/a^2}{20whG_{13}} \tag{14.15}$$

In the calculation of C_{SH}, the interlaminar shear modulus G_{13} is required. If G_{13} is unknown, the in-plane shear modulus, G_{12} (Chapter 7), can be used as an approximation to G_{13} for unidirectional composites. If the flexural modulus, E_1, of the ENF specimen is known, it is most straightforward to determine G_{IIC} from a beam theory expression [16],

$$G_{IIC} = \frac{9a^2\,P^2}{16w^2\,h^3\,E_1}\left[1 + 0.2\left(\frac{h}{a}\right)^2\frac{E_1}{G_{13}}\right] \tag{14.16}$$

To determine G_{IIC}(NL), G_{IIC}(vis.), and G_{IIC}(max.), the loads P(NL), P(vis.), and P(max.), defined in Figure 14.11, and the initial crack length are substituted in Equations (14.14) and (14.16). Consider, as an example, the load-displacement record shown in Figure 14.12 for a carbon/epoxy ENF specimen of dimensions L = 50.8 mm, a = 27.9 mm, 2h = 3.5 mm, w = 25.3 mm, and $G_{13} = G_{12} = 5$ GPa. The critical load was 762 N, and the specimen compliance was 2.3 μm/N. Substituting these data in Equations (14.14) and (14.15) gives $G_{IIC} = 553$ J/m^2.

Note that the experimental compliance calibration method may be used for determination of the fracture toughness of the ENF specimen [20,22]. This method requires long ENF specimens with long precrack lengths, which enable sliding of the specimen across the test fixture to cover the desired range of crack lengths. Compliance data are collected at each crack length

by loading the specimen at loads small enough not to promote crack extension. A set of compliance values at discrete crack lengths (a) is obtained, and the data set is fitted by a third-order polynomial in crack length,

$$C = C_0 + C_3 a^3 \tag{14.17}$$

Differentiation of this equation with respect to crack length, and substitution into Equation (2.59), yields

$$G = \frac{3P^2 C_3 a^2}{2w} \tag{14.18}$$

Substitution of the corresponding critical loads, Figure 14.11, into this equation yields G_{IIC}(NL), G_{IIC}(vis.), and G_{IIC}(max.).

Overall, however, this method tends to yield highly scattered G_{IIC} data for the ENF test. Davies et al. [23] found that the coefficient of variation for G_{IIC} as determined for a carbon/epoxy composite using Equation (14.18) is 21%, whereas the corresponding value for the beam analysis method, Equation (14.16), is 14%. The reasons for the low precision are that the rate of change in the ENF specimen compliance with crack length is relatively small, and the experimental determination of compliance requires accurate measurements of crack length, load, and displacement, whereas Equation (14.16) requires load and crack length only [23].

14.3 The Four-Point Bend ENF (4ENF) Test

As indicated above, the ENF specimen suffers from unstable crack growth, which means that only one toughness value per specimen can be determined. Consequently, it is not possible to determine Mode II R-curves using this specimen. In an effort to overcome this drawback, a stable test obtained by modification of the load introduction to the ENF specimen (Figure 14.13) was recently proposed by Martin and Davidson [24]. Because of the four-point loading, the specimen is called a 4ENF specimen [24]. The 4ENF test employs a specimen similar to the ENF specimen and is currently being examined as a standard pure Mode II delamination fracture test method by the ASTM D-30 committee. As discussed by Davies et al. [23], promoting stable delamination growth has several benefits; an R-curve can be determined, which may be important for damage tolerance assessment, and an R-curve yields more significance to the measured initiation value of G_{IIC}. The data analysis for the 4ENF specimen is currently based on the experimental compliance method because this method is perceived as being more accurate

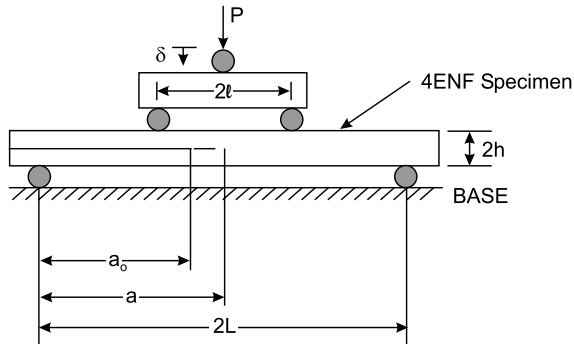

FIGURE 14.13
Principle of 4ENF test and definition of geometry parameters.

than analytically derived procedures. Presently, to the best knowledge of the authors, no beam analysis for the 4ENF specimen has been published.

14.3.1 4ENF Specimen Preparation

The 4ENF specimen is prepared in the same way as the ENF specimen, although the recommended length is 140 mm. The length of the insert film at the edge of the panel (Appendix B) should be about 50 mm. The ends of the insert should be marked on the edges of the panels before specimens are cut. After specimens are cut from the panels, measure the length of each specimen to the nearest millimeter. Measure the width and thickness of each specimen at the center and 1 cm from each end, to the nearest 0.05 mm. The variation in thickness should not exceed 0.1 mm. Similar to the DCB and ENF specimens, the edges of the specimens should be coated with a brittle white coating to aid in detection of the crack tip. Place a reference mark at the end of the insert. Its exact location is difficult to locate, but may be verified after completion of the fracture test by splitting the specimen open. Marks should be placed every mm over a distance of about 4 cm ahead of the insert tip.

14.3.2 4ENF Test Fixture

Figure 14.13 shows the pertinent geometry symbols for the 4ENF test geometry and specimen. The diameter of the loading and support cylinders are as specified for the three-point flexure test in ASTM D 790, i.e., 10 mm [21]. The lower support span, 2L, should be 10 cm, and the upper span, 2ℓ, should be 6 cm. The upper loading cylinders should be mounted on a beam that is allowed to rotate freely about a horizontal axis perpendicular to the longitudinal axis of the beam specimen to ensure equal load sharing for the two loading cylinders during loading of the (asymmetric) specimen. The upper cylinder, where load is introduced, should be centered between the upper and lower loading and support cylinders.

14.3.3 4ENF Test Procedure

The 4ENF specimen should be placed in the fixture so that the tip of the insert film, which is about 50 mm long, is 15 mm inside the left upper loading cylinder (Figure 14.13). This positioning corresponds to a 35-mm-long precrack length, $a_0 = 35$ mm. To facilitate positioning of the specimen in the test fixture at the proper crack length, it is beneficial to use a low-magnification (10×) traveling microscope. Mark the support location at the cracked end on the specimen edge to aid in subsequent crack length identification.

Load the specimen in a properly calibrated test fixture using displacement control. Set the crosshead rate between 0.1 and 0.5 mm/min and adjust the traveling microscope so that propagation of the delamination can be monitored during loading.

The displacement of the loading point, δ (Figure 14.13), can be measured using an LVDT or from the crosshead motion corrected for machine and fixture compliance, if necessary. Record the load (P) vs. displacement (δ) response on a chart recorder while observing the delamination front. At the onset of crack propagation, mark the P-δ graph as indicated by "vis" in Figure 14.14. The loading should be stopped after about 2 to 3 mm of crack growth. If possible, check the opposite edge for uniformity of growth. The difference in crack length between the two edges should be less than 2 mm for a valid test. Sometimes the crack propagates unstably from the insert. Figure 14.15 represents actual test results for an IM7/8552 carbon/epoxy 4ENF specimen [25]. For the first increment the crack "jumped" about 12 mm (Figure 4.15). Schuecker and Davidson [25] attributed this phenomenon to the higher toughness associated with propagation through the resin pocket in front of the insert film.

After 2 to 3 mm of crack growth is observed, the specimen should be completely unloaded at a crosshead rate up to 5 mm/min. The specimen should then be reloaded at the same rate as used for the first loading increment. If a significant amount of unstable growth occurs, Schuecker and Davidson [25] propose to shift the specimen to the left in the fixture so that

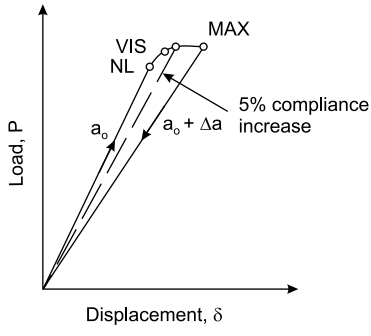

FIGURE 14.14
Schematic load-displacement record for 4ENF test.

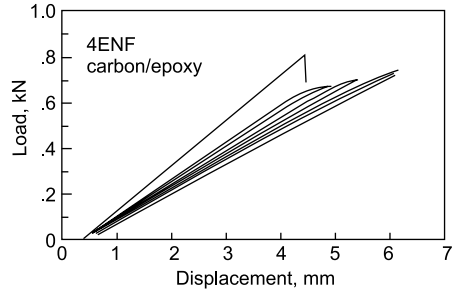

FIGURE 14.15
Load-displacement curves for a carbon–epoxy 4ENF specimen showing initial unstable growth [25].

the original initial crack length is restored. This is necessary to enable enough length for subsequent crack propagation increments (at least six). Following this procedure, subsequent propagation cycles, each with 2 to 3 mm of crack propagation, should be performed in the above-described manner (Figure 14.15) until the delamination front reaches within 10 mm of the right loading cylinder. The subsequent crack increments should occur in a stable manner without crack jumps.

After completion of the test, remove the specimen from the fixture and split it open. The length of the precrack can now be measured, which, if necessary, enables for correction of the crack length, a, measured from the marks on the specimen edge.

14.3.4 4ENF Data Reduction

Evaluation of the fracture toughness, G_{IIC}, of the 4ENF specimen is based on the experimental compliance method. Compliance, $C = \delta/P$, is determined from the linear slope of the load-displacement record. After the crack lengths are corrected (see Section 14.3.3), compliance data are graphed as shown in Figure 14.16. As indicated in Figure 14.16, the C vs. a data follow a linear relation, i.e.,

$$C = C_0 + C_1 a \tag{14.19}$$

Combining Equations (14.19) and (14.2) yields

$$G = \frac{P^2 C_1}{2w} \tag{14.20}$$

where w is the specimen width. At fracture, $P = P_c$ and $G = G_{IIC}$. The parameter C_1 in Equations (14.19) and (14.20) is identified as the slope, m, of the line fitted to the data points in Figure 14.16. It is possible to determine fracture

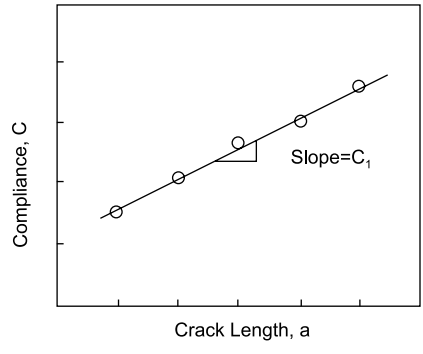

FIGURE 14.16
Schematic of compliance vs. crack length for a 4ENF specimen.

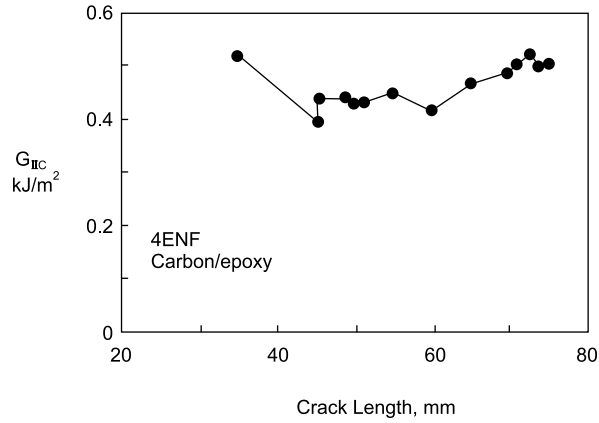

FIGURE 14.17
Mode II R-curve for a carbon/epoxy composite [23].

toughness values based on the load when the load-displacement record deviates from linearity (NL), the load when crack propagation is visually observed (vis.), and the maximum load (max.) (Figure 14.14). In case the P-δ record is highly nonlinear and there is no clear indication of an early maximum, the point on the P-δ curve where a straight line offset by a 5% increase in compliance intersects the curve may be used as the maximum load (Figure 14.15). In this manner, it is possible to establish three toughness values for each loading increment, i.e., G_{IIC}(NL), G_{IIC}(vis.), and G_{IIC}(max.). If any of these toughness values are plotted vs. crack length, a fracture resistance curve is obtained. Figure 14.17 shows an R-curve determined for a carbon/epoxy composite where G_{IIC}(max.) is plotted vs. crack extension [23]. The first data point represents (unstable) propagation from the insert. The R-curve for stable growth is quite flat, although there is a slight increase in G_{IIC} with crack extension for this composite. The initial G_{IIC} value tends to be 20 to 30% higher than those at subsequent crack increments [23,25]. Moreover, the G_{IIC} values determined using the 4ENF test are typically 10 to 20% higher than those determined using the ENF test [26]. Part of this difference has been attributed to friction between sliding crack faces, which is more a concern for the 4ENF test than the ENF test. This is because in the 4ENF test there are two contact regions where the crack faces slide (Figure 14.13), whereas in the ENF geometry (Figure 14.8) there is only one such region. Detailed analysis of the frictional effect in the 4ENF test [26], however, shows that in a typical 4ENF test, friction will increase the apparent G_{IIC} value by no more than 5%.

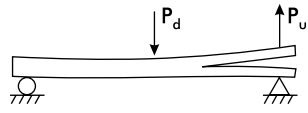

FIGURE 14.18
Principle of MMB test.

14.4 Mixed-Mode Bending (MMB) Test

In most practical situations, delaminations in composite laminates tend to grow in mixed-mode stress fields, i.e., tension and shear stresses are acting ahead of the crack front. Previous work, e.g., References [27,28], has shown that the resistance to delamination growth increases as the amount of shear loading (Mode II) increases. Consequently, delamination characterization requires mixed-mode fracture testing. Several mixed-mode fracture tests exist where various combinations of Mode I and Mode II can be generated. Most such methods, however, suffer from complicated test fixturing, a small range of mode mixities (G_{II}/G_I), and varying mode mixity as the crack grows [29].

The most promising test principle for mixed-mode delamination toughness testing is the MMB test proposed by Crews and Reeder [30–32] (Figure 14.18). The MMB test is a superposition of the DCB and ENF tests discussed previously. The MMB method has recently become an ASTM standard [33] because of simplicity of testing and the wide range of mode mixities possible.

Figure 14.19 depicts the geometry parameters and test principle of the MMB specimen. The loading lever adds an opening load to the midspan-loaded ENF specimen. The distance, c, between the point of load application and the midspan, determines the ratio of the downward force, P_d, to upward force, P_u, and hence the mode mixity. Pure Mode II corresponds to c = 0, with the ratio G_{II}/G_I decreasing with increasing distance c.

A distance of 15 mm between the point of load application and the specimen midplane (Figure 14.19) has been found to minimize geometrical nonlinearity effects [31,32]. Figure 14.20 shows various parts of the MMB assembly [34]. Detailed drawings are provided in ASTM Standard D 6671 [33]. Loading supports should be between 5 and 15 mm in diameter and should be mounted on roller bearings. The MMB specimen is loaded through roller bearings attached to the lever (Figure 14.20). Figure 14.21 shows a photograph of the MMB test setup. The loading lever is a low weight aluminum I-beam that is several orders of magnitude stiffer than the specimen.

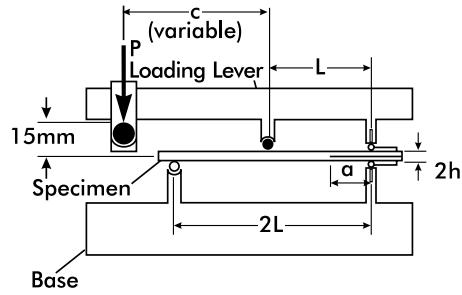

FIGURE 14.19
Definition of geometry parameters for the MMB specimen.

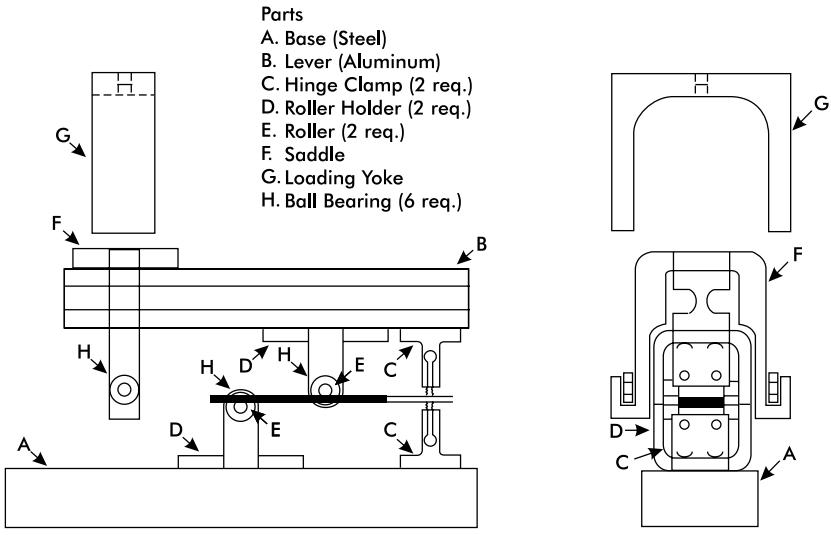

FIGURE 14.20
MMB test assembly [33].

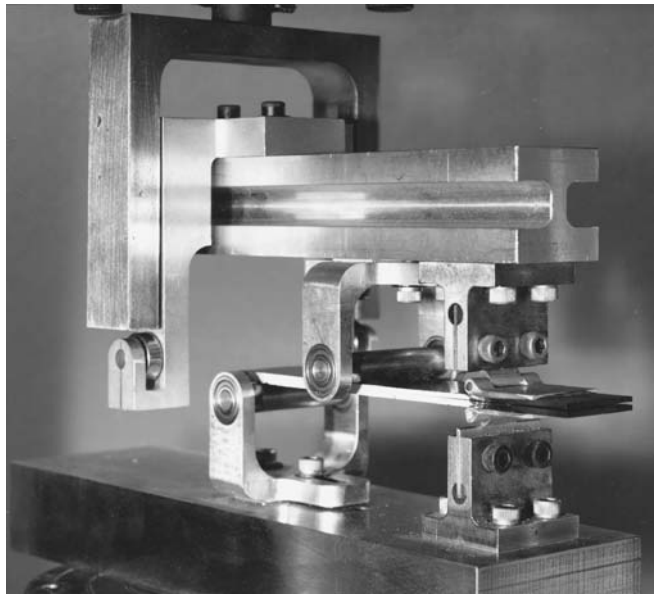

FIGURE 14.21
MMB test setup. (Courtesy of J.R. Reeder, NASA Langley Research Center.)

The lever load, the midspan load, and the left support reaction are applied through bearing-mounted rollers to reduce frictional forces. The right end of the specimen is loaded through high-quality, extruded aluminum hinges bonded to the specimen arms. The apparatus rests on a thick steel base.

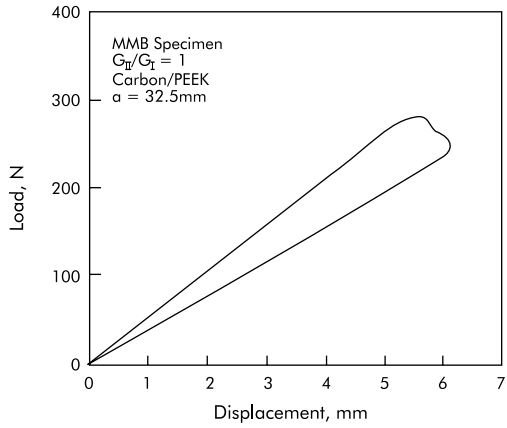

FIGURE 14.22
Load-displacement record for a carbon/PEEK MMB specimen [30].

14.4.1 MMB Test Procedure

The MMB test employs a 165-mm-long, hinged specimen prepared as the DCB specimen discussed in Section 14.1 (no precrack) (see also Appendix B). The width and thickness of each specimen is measured to the nearest 0.025 mm at the midpoint and at 1 cm from both ends. Three thickness measurements are made at each of these positions with one measurement close to each edge and one at the center. Variations in thickness should not exceed 0.1 mm. Average values of the width and thickness measurements shall be recorded. The specimen width, w, and nominal thickness, 2h, for the carbon/epoxy composite considered by Reeder and Crews [30–32] are 25 mm, and 3 to 4.4 mm, respectively. The initial delamination length, a, is 25 mm, and the half-span length, L, is 50 mm (Figure 14.19). The loading lever length, c, should be set to approximately achieve the following mode mixities: G_{II}/G_I = 0.25, 1, and 4 (using Equation (4.25) of the next section). Test a minimum of three replicate specimens at each mode mixity.

Use a crosshead rate of 0.5 mm/min for consistency with the Mode I and Mode II tests discussed above. Record the load-displacement response on an x-y recorder, while monitoring the crack tip with a low magnification traveling microscope. If slow, stable crack growth occurs, mark this event on the load-displacement curve. Figure 14.22 shows a load-displacement record for a carbon/PEEK composite [30]. It is observed that the load-displacement record is similar to that of the ENF specimen, Figure 14.11, which allows evaluation of G_C(NL), G_C(vis.), and G_C(max.).

14.4.2 MMB Data Reduction

The following empirical expressions for the Mode I and Mode II components of the strain energy release rate were suggested by Hashemi et al. [34] and Kinloch et al. [35],

$$G_I = \frac{12P_I^2(a + xh)^2}{w^2h^3E_1} \tag{14.21a}$$

$$G_{II} = \frac{9P_{II}^2(a + 0.42xh)^2}{16w^2h^3E_1} \tag{14.21b}$$

where $G = G_I + G_{II}$, and P_I and P_{II} are the opening and shearing components of the applied load given by [30],

$$P_I = P\left(\frac{3c - L}{4L}\right) \tag{14.22a}$$

$$P_{II} = \frac{P(c + L)}{L} \tag{14.22b}$$

The correction term x in Equations (14.21) was obtained by curve fitting Equations (14.21) to numerical (finite element) data [34,35],

$$x = \left[\frac{E_1}{11G_{13}}\left(3 - 2\left(\frac{\Gamma}{\Gamma + 1}\right)^2\right)\right]^{1/2} \tag{14.23}$$

with

$$\Gamma = 1.18\frac{\sqrt{E_1E_2}}{G_{13}} \tag{14.24}$$

The expressions (14.21) are considered quite accurate for commonly used MMB geometries and carbon/epoxy composites [36]. It may furthermore be verified that the ratio between the fracture modes, e.g., G_{II}/G_I, as given by Equations (14.21), is only weakly dependent on crack length.

An approximate equation for the mode mixity is obtained from the asymptotic beam analysis presented in Reference [30],

$$\frac{G_{II}}{G_I} = \frac{3}{4}\left(\frac{c + L}{3c - L}\right)^2, \qquad c \geq L/3 \tag{14.25}$$

For $c < L/3$, crack face contact may occur that corresponds to $G_1 = 0$ and invalidates the analysis above. Equation (14.25) can be used for initial (approximate) calculation of the mode mixity, which more accurately is calculated using Equations (14.21).

After testing is complete, break open the specimen and measure the crack length (the distance from the center of the hinge pin to the end of the delamination starter film). Measure the crack length at the edges and center of the specimen and obtain a mean value.

Calculations of G_I and G_{II} using Equations (14.21) require the critical load and several of the material properties, i.e., E_1, E_2, and G_{13}. The moduli E_1, E_2, and G_{13} (approximately equal to G_{12}) have to be known from previous tests (Chapters 5 and 7). The (flexural) modulus E_1 may also be calculated from the MMB compliance C [33, 37]

$$E_1 = \frac{8(3c - L)^2(a + xh)^3 + (c + L)^2\left[4L^3 + 6(a + 0.42xh)^3\right]}{16CL^2wh^3} \tag{14.26}$$

where C is the specimen compliance corrected for the load cell compliance and (lever length-dependent) fixture compliance.

As an alternative, more accurate procedure, the uncracked portion of the beam may be tested in three-point bending [21] to obtain the flexural modulus E_1 as specified in Chapter 8.

The components $(G_I, G_{II})_C$ of the mixed-mode fracture toughness are calculated using the various moduli, specimen geometry data, and measured critical load in Equations (14.21).

It has become customary to represent mixed-mode fracture toughness data in terms of the Mode II fraction, G_{II}/G, where $G = G_I + G_{II}$. Benzeggagh and Kenane [38] proposed the following type of equation for empirical description of the relation G_C vs. G_{II}/G,

$$G_C = G_{IC} + \left(G_{IIC} - G_{IC}\right)\left(G_{II}/G\right)^{\beta} \tag{14.27}$$

where β is an empirical factor determined from a fit of the experimentally determined G_C vs. G_{II}/G data. Figure 14.23 shows the relation between G_C and G_{II}/G for a range of carbon fiber, polymer matrix composites [37]. It is observed that the fracture toughness of AS4/PEEK remains fairly independent of mode ratio, while the fracture toughness of the more brittle thermoset-matrix composites shows a quite large sensitivity to the mode ratio.

14.5 Edge-Cracked Torsion (ECT) Test

The ECT test was introduced by Lee in 1993 [39] as a test method to determine the Mode III delamination toughness of composites. Figure 14.24 shows the ECT test specimen and test fixture. The test specimen is a rectangular composite plate containing an edge delamination at the midplane.

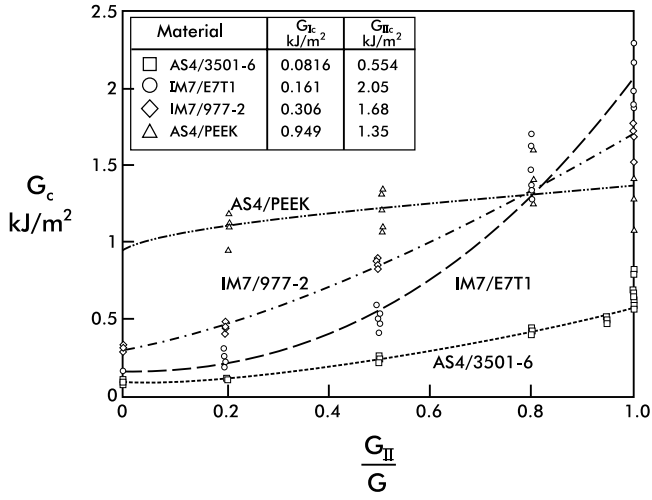

FIGURE 14.23

Mixed-mode interlaminar fracture toughness for a variety of carbon fiber, polymer matrix composites. The parameter β (Equation (14.27)) varies from 0.63 (AS4/PEEK) to 2.35 (IM7/977-2) for such composites [37].

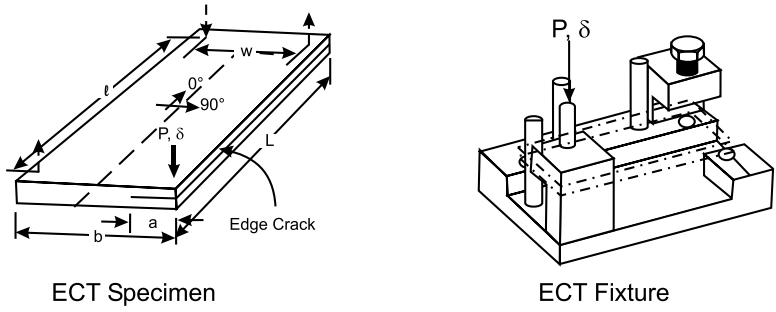

FIGURE 14.24

ECT specimen and test fixture [39]. The specimen is loaded near the right front corner and supported near the other corners. Forces at those corners are reaction forces.

For carbon/epoxy, a lay-up of $[90/(\pm 45)_n/(\mp 45)_n/90]_s$, with the longitudinal direction defining the 0° direction, is recommended. The integer n is 2 or 3, corresponding to a total of 20 or 28 unidirectional plies, respectively. A precrack is defined by inserting a strip of film of thickness less than 13 μm between the 90° plies at the midplane of the panel to define an edge crack of length a (Figure 14.24). Appendix B outlines the panel design for the ECT specimen.

The test fixture (Figure 14.24) is designed so that three corners of the panel are supported, while one corner on the cracked side is displaced normal to the panel. This loading produces a pair of couples of equal magnitude but of opposite sign that induce twisting of the plate and the characteristic Mode III deformation illustrated in Figure 2.9. Crack propagation should

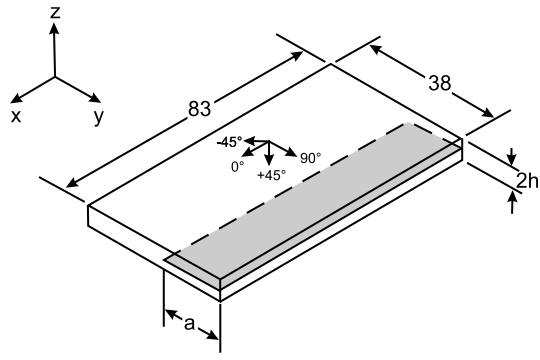

FIGURE 14.25
ECT specimen geometry and dimensions.

ideally occur uniformly in a direction perpendicular to the crack front at the midplane, i.e., parallel to the 0° fibers. In this way, a toughness value, G_{IIIC}, is determined that may be compared to those determined in the Mode I and Mode II tests outlined above.

14.5.1 ECT Specimen Preparation

The ECT specimen (Figure 14.25) is a flat, rectangular plate, 83 mm long and 38 mm wide. Lay-ups are $[90/(\pm 45)_n/(\mp 45)_n/90]_s$, where n = 2 or 3 for unidirectional carbon/epoxy and n = 3 for unidirectional glass/epoxy. Corresponding laminate thicknesses are about 2.5 and 3.6 mm. An edge crack is defined by inserting a thin strip (<13 μm) of nonstick film such as Teflon, Kapton, or polypropylene. The film is inserted between the 90° plies at the midplane to define a straight precrack of the desired length, a (Figure 14.25). Specimen details are provided in Figure 14.25. Panel design is outlined in Appendix B. Precrack lengths of 0, 8, 11, 15, 19, and 23 mm are recommended. Although testing of the uncracked specimen (a = 0) does not yield any toughness data, it provides a reference point for subsequent data reduction using the compliance calibration method. After the specimens are cut from the panel, measure the width (b) and length (L) to the nearest 0.1 mm, and thickness (2h) to the nearest 0.01 mm of each specimen. Measure the width and length near the corners and at the midlength of each side. Measure thickness at the center and near each corner. Thickness should not vary more than 0.1 mm. In a manner similar to that for the other fracture specimens, the free edges may be coated with a brittle white coating to aid in visual detection of crack extension.

14.5.2 ECT Test Fixture

The schematic in Figure 14.24 shows that the ECT specimen is constrained against lateral displacement at three corners and loaded by a concentrated

normal force at the forth corner. The distance, w, between the support–loading pins along the short edge is 31.8 mm. The distance, ℓ, between the support–loading pins along the crack front is 76.2 mm.

14.5.3 ECT Test Procedure

Place the ECT test specimen in the test fixture. Adjust the threaded support pin (Figure 14.24) so that all four support–loading pins contact the specimen. Place the fixture in a properly calibrated load frame. Set the crosshead rate at 1.3 mm/min, and load the specimen while recording the load (P) vs. displacement (δ) response on an x-y recorder. Observe the crack front and P-δ record for indications of propagation of the crack.

Figure 14.26 shows schematic load-displacement records that are typically observed for the ECT test. The curve in Figure 14.26(a) indicates stable crack propagation under increasing load, whereas the curve in Figure 14.26(b) indicates some extent of unstable growth and a clearly defined early maximum load, P_c. For the curve in Figure 14.26(a), the critical load for crack propagation, P_c, is determined by the 5% offset method. A straight line offset by a 5% increase in compliance is drawn as shown in Figure 14.26(a), and P_c is defined as the load value where this line intersects the recorded P-δ curve. Notice that if the 5% offset line intersects the P-δ curve after the maximum load is reached, as in Figure 14.26(b), P_c is defined as the maximum load.

After completion of the fracture test, unload the specimen, and remove it from the fixture. Separate the fracture specimen into two halves. This enables accurate measurements of the precrack length (Figure 14.25) at the edges and midlength of the crack front. Although the final crack length is not used in the determination of G_{IIIC}, an average crack length may be determined from crack length measurements at six or more equally spaced locations along the crack front.

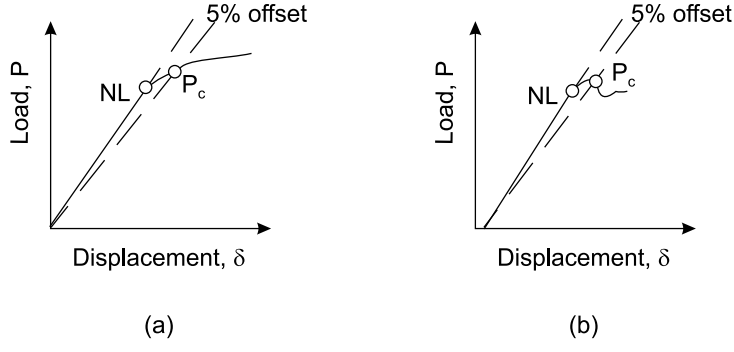

FIGURE 14.26
Schematic illustrations of load-displacement records and determination of critical load, P_c, for crack propagation in the ECT specimen: (a) stable growth, and (b) initial unstable growth.

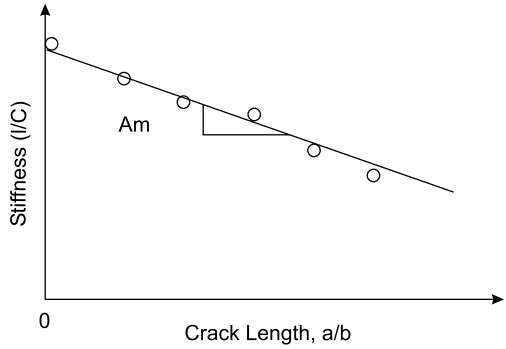

FIGURE 14.27
Stiffness (1/C) of ECT specimen plotted vs. normalized crack length (a/b) for experimental determination of mode III toughness.

14.5.4 ECT Data Reduction

Evaluation of the Mode III fracture toughness, G_{IIIC}, of the ECT specimen is based on the experimental compliance calibration method. Compliance, C, is determined from the linear slope of the load vs. displacement record (Figure 14.26), $C = \delta/P$. After correction for machine and fixture compliance, the stiffness, P/δ, i.e., the inverse of the compliance, is plotted vs. the average initial crack length, a, normalized by edge length, b, for all the specimens tested (Figure 4.27). Analysis of the ECT test [39] predicts a linear dependence of specimen stiffness on crack length, which is also observed experimentally (Figure 4.28) [40]. A linear equation in crack length is fitted to the stiffness data in Figure 14.27 using the least-squares method according to

$$\frac{1}{C} = A\left[1 - m\left(\frac{a}{b}\right)\right] \tag{14.28}$$

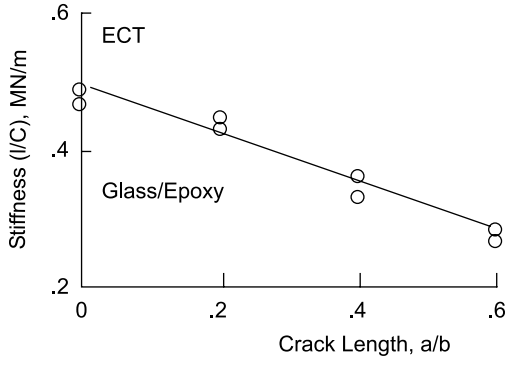

FIGURE 14.28
Stiffness vs. crack length data for glass/epoxy ECT specimen [40].

where A is the intercept of the line at the 1/C axis, and Am is the magnitude of the slope of the line. Differentiation of Equation (14.28) yields, in conjunction with (14.2), the strain energy release rate for the ECT specimen

$$G = \frac{mCP^2}{2Lb\left(1 - m\left(a/b\right)\right)} \tag{14.29}$$

where L is the distance between the two couples defined in Figure 14.24. Substitution of the critical load, P_c, into the above equation yields the Mode III delamination toughness, G_{IIIC}. Similar to the other delamination tests, G_{IIIC}(NL) and G_{IIIC}(max.) may be determined on the basis of the load-displacement record (Figure 14.26). For example, Li et al. [40] determined G_{IIIC} for a glass/epoxy composite with 56% fiber volume fraction and found G_{IIIC}(NL) = 1.23 ± 0.09 kJ/m² and G_{IIIC}(max.) = 1.48 ± 0.18 kJ/m².

References

1. R.B. Pipes and N.J. Pagano, Interlaminar stresses in composite laminates under uniform axial extension, *J. Compos. Mater.*, 4, 538–548, 1970.
2. D.J. Nicholls and J.P. Gallagher, Determination of G_{IC} in angle-ply composites using a cantilever beam test method, *J. Reinf. Plast. Compos.*, 2, 2–17, 1983.
3. P. Robinson and D.Q. Song, A modified DCB specimen for mode I testing of multidirectional laminates, *J. Compos. Mater.*, 26, 1554–1577, 1992.
4. Y.B. Shi, D. Hull, and J.N. Price, Mode II fracture of +θ/–θ angled laminate interfaces, *Compos. Sci. Technol.*, 47, 173–184, 1993.
5. F. Ozdil and L.A. Carlsson, Mode I interlaminar fracture of interleaved graphite/epoxy, *J. Compos. Mater.*, 26, 432–459, 1992.
6. N. Alif, L.A. Carlsson, and J.W. Gillespie, Jr., Mode I, mode II, and mixed mode interlaminar fracture of woven fabric carbon/epoxy, *ASTM Spec. Tech. Publ.*, 1242, 82–106, 1997.
7. B.N. Cox, R. Massabo, D.R. Mumm, A. Turrettini, and K.B. Kedward, Delamination Fracture in the Presence of Through-Thickness Reinforcement, *Proceedings of the 11th International Conference on Composite Matererials* (ICCM-11), M.L. Scott, Ed., Gold Coast, Australia, 1997, Technomic, Lancaster, PA, 1997, pp. 159–177.
8. ASTM Standard D5528-94a, *Test Method for Mode I Interlaminar Fracture Toughness of Unidirectional Fiber-Reinforced Polymer Matrix Composites*, American Society for Testing and Materials, West Conshohocken, PA, 2001.
9. W.D. Bascom, R.J. Bitner, R.J. Moulton, and A.R. Siebert, The interlaminar fracture of organic-matrix woven reinforced composites, *Composites*, 11, 9–18, 1980.
10. D.J. Wilkins, J.R. Eisenmann, R.A. Camin, W.S. Margolis, and R.A. Benson, Characterizing delamination growth in graphite-epoxy, *ASTM Spec. Tech. Publ.* 775, 168–183, 1982.
11. Z. Suo, G. Bao, and B. Fan, Delamination R-curve phenomnena due to damage, *J. Mech. Phys. Solids*, 40, 1–16, 1992.

12. T.K. O'Brien and R.H. Martin, Results of ASTM round robin testing for mode I interlaminar fracture toughness of composite materials, *J. Compos. Tech. Res.*, 15, 269–281, 1993.
13. J.P. Berry, Determination of fracture energies by the cleavage technique, *J. Appl. Phys.*, 34, 62–68, 1963.
14. A.J. Russell and K.N. Street, Factors affecting the interlaminar fracture energy of graphite/epoxy laminates, in *Progress in Science and Engineering of Composites*, T. Hayashi, K. Kawata, and S. Umekawa, Eds., ICCM-IV, ASM International, Tokyo, 1982, pp. 279–286.
15. A.J. Russell and K.N. Street, Moisture and temperature effects on the mixed-mode delamination fracture of unidirectional graphite/epoxy, *ASTM Spec. Tech. Publ.*, 876, 349–370, 1985.
16. L.A. Carlsson, J.W. Gillespie, Jr., and R.B. Pipes, On the analysis and design of the end notched flexure (ENF) specimen for mode II testing, *J. Compos. Mater.*, 20, 594–604, 1986.
17. J.W. Gillespie, Jr., L.A. Carlsson, and R.B. Pipes, Finite element analysis of the end notched flexure (ENF) specimen for measuring mode II fracture toughness, *Compos. Sci. Technol.*, 26, 177–197, 1986.
18. AECMA Aerospace Series, Carbon Fiber Reinforced Plastics: Determination of Interlaminar Fracture Toughness Energy in Mode I — G_{IC} (prEN6033) and Mode II — G_{IIC} (pr EN 6034), Association Europeene de Constructeurs de Materiel Aerospatial, Paris, France, Dec. 1995.
19. Japan Industrial Standards, JIS 7086, *Testing Methods for Interlaminar Fracture Toughness of Carbon Fiber Reinforced Plastics*, Japanese Standards Association, Tokyo, Japan, 1993.
20. T.K. O'Brien, G.B. Murri, and S.A. Salpekar, Interlaminar shear fracture toughness and fatigue thresholds for composite materials, *ASTM Spec. Tech. Publ.*, 1012, 222–250, 1989.
21. ASTM Standard D 790-00, *Test Methods for Flexural Properties of Unreinforced and Reinforced Plastics and Electrical Insulating Materials*, American Society for Testing and Materials, West Conshohocken, PA, 2002.
22. L.A. Carlsson, J.W. Gillespie, Jr., and B.R. Trethewey, Mode II interlaminar fracture of graphite/epoxy and graphite/PEEK, *J. Reinf. Plast. Compos.*, 5, 170–187, 1986.
23. P.D. Davies, G.D. Sims, B.R.K. Blackman, A.J. Brunner, K. Kageyama, M. Hojo, K. Tanaka, G. Murri, C. Rousseau, B. Gieseke, and R.H. Martin, Comparison of test configurations for determination of mode II interlaminar fracture toughness results from international collaborative test programme, *Plast. Rubber Compos.*, 28(8), 432–437, 1999.
24. R.H. Martin and B.D. Davidson, Mode II fracture toughness evaluation using a four point bend end notched flexure test, *Plast. Rubber Compos.*, 28(8), 401–406, 1999.
25. C. Shuecker and B.D. Davidson, Evaluation of the accuracy of the four-point end-notched flexure test for mode II delamination toughness determination, *Compos. Sci. Technol.*, 60, 2137–2146, 2000.
26. C. Schuecker and B.D. Davidson, Effect of friction on the perceived mode II delamination toughness from three- and four-point end-notched flexure tests, *ASTM Spec. Tech. Publ.*, 1383, 334–344, 2000.
27. W.S. Johnson and P.D. Mangalgiri, Influence of the resin on interlaminar mixed mode fracture, *ASTM Spec. Tech. Publ.*, 937, 295–315, 1987.

28. S. Hashemi, A.J. Kinloch, and J.G. Williams, The effects of geometry, rate, and temperature on the mode I, mode II, and mixed mode I/II interlaminar fracture of carbon-fiber/poly (ether-ether ketone) composites, *J. Compos. Mater.*, 24, 918–956, 1990.
29. L.A. Carlsson, Fracture of fiber composites, in *Structure and Properties of Composites*, T.-W. Chou, Ed., VCH Publishers, Weinheim, Germany, 1993, pp. 533–582.
30. J.R. Reeder and J.H. Crews, Jr., Mixed mode bending method for delamination testing, *AIAA J.*, 28(7), 1270–1276, 1990.
31. J.R. Reeder and J.H. Crews, Jr., Redesign of the mixed mode bending test for delamination toughness, S.W. Tsai and G.S. Springer, Eds., *Proceedings of the 8th International Conference on Composite Matererials*, Honolulu, HI, July 1991, Society for the Advancement of Materials and Process Engineering (SAMPE), Covina, CA.
32. J.R. Reeder and J.H. Crews, Jr., Redesign of the mixed mode bending delamination test to reduce nonlinear effects, *J. Compos. Technol. Res.*, 14(1), 12–19, 1992.
33. ASTM Standard D 6671-01, *Test Method for Mixed Mode I-Mode II Interlaminar Fracture Toughness of Unidirectional Fiber Reinforced Polymer Matrix Composites*, American Society for Testing and Materials, West Conshohocken, PA, 2001.
34. S. Hashemi, A.J. Kinloch, and J.G. Williams, The analysis of the interlaminar fracture in uniaxial fiber-polymer composites, *Proc. Math. Phys. Sci.*, 427, 173–199, 1990.
35. A.J. Kinloch et al., The mixed-mode delamination of fiber composite materials, *Compos. Sci. Tech.*, 47, 225–237, 1993.
36. S. Bhashyan and B.D. Davidson, An evaluation of data reduction methods for the mixed-mode bending test, *Proc. 37th Struct., Struct. Dyn. and Mater. Conf.*, AIAA-96-1419-CP, 1996.
37. J.R. Reeder, personal communication.
38. M.L. Benzeggagh and M. Kenane, Measurement of mixed-mode delamination fracture toughness of unidirectional glass/epoxy composites with mixed-mode bending apparatus, *Compos. Sci. Tech.*, 56, 439–449, 1996.
39. S.M. Lee, An edge crack torsion method for mode III delamination fracture testing, *Compos. Technol. Res.*, 15(3), 193–201, 1993.
40. X. Li, P. Davies, and L.A. Carlsson, Influence of fiber volume fraction on mode III interlaminar toughness of glass/epoxy, to be published.